Apolipoprotein A-I helical structure and stability in discoidal high-density lipoprotein (HDL) particles by hydrogen exchange and mass spectrometry

Palaniappan Sevugan Chetty[a], Leland Mayne[b], Zhong-Yuan Kan[b], Sissel Lund-Katz[a], S. Walter Englander[b,1], and Michael C. Phillips[a,1]

[a]Lipid Research Group, Gastroenterology, Hepatology and Nutrition Division, Children's Hospital of Philadelphia, Philadelphia, PA 19104-4318; and [b]The Johnson Research Foundation, Department of Biochemistry and Biophysics, Perelman School of Medicine at the University of Pennsylvania, Philadelphia, PA 19104-4318

Contributed by S. Walter Englander, June 4, 2012 (sent for review February 24, 2012)

To understand high-density lipoprotein (HDL) structure at the molecular level, the location and stability of α-helical segments in human apolipoprotein (apo) A-I in large (9.6 nm) and small (7.8 nm) discoidal HDL particles were determined by hydrogen-deuterium exchange (HX) and mass spectrometry methods. The measured HX kinetics of some 100 apoA-I peptides specify, at close to amino acid resolution, the structural condition of segments throughout the protein sequence and changes in structure and stability that occur on incorporation into lipoprotein particles. When incorporated into the large HDL particle, the nonhelical regions in lipid-free apoA-I (residues 45–53, 66–69, 116–146, and 179–236) change conformation from random coil to α-helix so that nearly the entire apoA-I molecule adopts helical structure (except for the terminal residues 1–6 and 237–243). The amphipathic α-helices have relatively low stability, in the range 3–5 kcal/mol, indicating high flexibility and dynamic unfolding and refolding in seconds or less. A segment encompassed by residues 125–158 exhibits bimodal HX labeling indicating co-existing helical and disordered loop conformations that interchange on a time scale of minutes. When incorporated around the edge of the smaller HDL particle, the increase in packing density of the two apoA-I molecules forces about 20% more residues out of direct contact with the phospholipid molecules to form disordered loops, and these are the same segments that form loops in the lipid-free state. The region of disc-associated apoA-I that binds the lecithin-cholesterol acyltransferase enzyme is well structured and not a protruding unstructured loop as reported by others.

atherosclerosis | amphipathic α-helix | protein secondary structure

There is great interest in understanding the structure—function relationships of high-density lipoprotein (HDL) because of its important antiatherogenic properties. Because high-resolution structures of HDL microemulsion particles cannot be obtained by current X-ray crystallography and NMR methods, alternative biophysical approaches have been used to characterize various subspecies of HDL. Structural models that show the general lipid and protein organization in HDL particles are now available (for reviews, see refs. 1–6). To derive detailed understanding at the molecular level of how HDL functions in cholesterol transport (7) and in reducing the incidence of premature cardiovascular disease (8), higher-resolution structural information is required.

Reconstituted discoidal HDL particles that are models of nascent HDL (9) created by the interaction of apolipoprotein (apo) A-I (3, 10), the principal protein of HDL, with the cell-surface ATP binding cassette transporter (ABCA1) (11, 12) have received a great deal of attention. A major advantage of model particles is the possibility of obtaining preparations that are sufficiently homogeneous for detailed structural investigation. The structure of a discoidal HDL particle (approximately 10 nm hydrodynamic diameter) comprising a 160-molecule segment of phospholipid (PL) bilayer stabilized by two apoA-I molecules has been modeled in detail. In the "double-belt" model, the apoA-I molecules are packed around the edge of the disc in an antiparallel orientation with their amphipathic α-helical segments (13) interacting with the PL acyl chains (14). This extended belt-like organization of the apoA-I molecules is derived from a similar conformation observed in the crystal structure of a lipid-free, N-terminal truncated variant of human apoA-I in which the molecule forms a horseshoe-shaped, pseudo-continuous, amphipathic α-helix (15). This structure is also consistent with a recent 2.2 Å-resolution crystal structure of a lipid-free C-terminally truncated apoA-I molecule (16).

This paper describes the detailed secondary structure for the complete human apoA-I molecule in discoidal HDL particles of different sizes. These particles of discrete size (7.8- and 9.6-nm hydrodynamic diameter) contain two apoA-I molecules and have the characteristics of naturally occurring nascent HDL particles. Such structural information will help provide an answer to the intriguing question of why apoA-I interacts with PL in a quantized fashion to stabilize HDL particles of defined size rather than to form a continuum of particle sizes. We applied hydrogen exchange (HX) and mass spectrometry (MS) methods (17–19) to determine the location, stability, and dynamics of α-helical segments within lipid-bound apoA-I molecules. This high-resolution structural information provides a basis for understanding the molecular interactions in which HDL particles participate.

Results

HDL Particle Characteristics. Reconstituted HDL particles containing approximately 70/1 and 28/1 mol/mol palmitoyl-oleoyl phosphatidylcholine (POPC) and human apoA-I (20) were employed in the hydrogen-deuterium exchange (HX) experiments. These HDL particles contain two apoA-I molecules and are homogeneous with hydrodynamic diameters of 9.6 and 7.8 nm, respectively (Fig. S1); such HDL particles have been characterized extensively (for reviews, see refs. 5, 21). The particles have been visualized by electron microscopy and are stable for prolonged periods when stored at 4 °C (22) and do not rearrange under the conditions of the HX experiments. In agreement with prior work, the apoA-I in these HDL particles is highly α-helical; analysis of CD spectra (Fig. S2) indicates that the helix content is approximately 80% compared to 52% for apoA-I in the lipid-free state.

Author contributions: P.S.C., S.L.-K., S.W.E., and M.C.P. designed research; P.S.C. and S.L.-K. performed research; Z.-Y.K. contributed new reagents/analytic tools; P.S.C., L.M., and Z.-Y.K. analyzed data; and P.S.C., S.W.E., and M.C.P. wrote the paper.

The authors declare no conflict of interest.

Freely available online through the PNAS open access option.

[1]To whom correspondence may be addressed. E-mail: engl@mail.med.upenn.edu or phillipsmi@email.chop.edu.

This article contains supporting information online at www.pnas.org/lookup/suppl/doi:10.1073/pnas.1209305109/-/DCSupplemental.

Analysis of HDL Particle HX. Previously we employed HX and mass spectrometry (MS) to define the positions and stabilities of hydrogen-bonded (α-helical) structures in the lipid-free apoA-I molecule (19). This involved determining the HX rates of amide hydrogens at known positions throughout the protein and comparing them to the exchange rate expected for the unstructured polypeptide (23, 24). As an example, Fig. 1 illustrates results for an apoA-I peptide (encompassing residues 159–180) within the 9.6-nm discoidal HDL particle. The measured time courses of HX (pD 7.3, 5 °C) for the approximately 100 apoA-I peptide fragments are presented in Fig. S3. Consistent with our previous work (19), many segments in lipid-free apoA-I form HX-protected α-helices (residues 7–44, 54–65, 70–78, 81–115, and 147–178), while the C-terminal length from residue 181 to 243 is in a disordered state. In the 9.6-nm discoidal HDL particle (Fig. S3) all segments exhibit protection against HX, indicating a widespread change in conformation from random coil to α-helix; in particular, segments 115–126, 127–158, 181–189, 190–213, 212–225, 226–232, and 231–243 undergo this change in conformation upon lipid binding. The protection factors (Pf) (see *Materials and Methods*) found for all the lipid-bound peptide fragments are listed in Table S1 (pD 7.3, 5 °C). Pf reports the slowing of HX rate relative to the rate for the same residues when they are present in random coil. Apart from N-terminal peptides spanning residues 1–16 and C-terminal peptides spanning residues 220–243, the peptide HX kinetics are well-described by a mono-exponential rate equation and a single Pf value > 50, consistent with each segment forming a helix of uniform but rather low stability that repeatedly experiences reversible cooperative unfolding, thereby modulating the measurable HX reaction (19). Peptides in the region of residues 127–158 exhibit bimodal HX kinetics and are discussed separately below. The far N- and C-terminal peptides exhibit HX kinetics that are best fitted by a bi-exponential rate equation indicating that some amide hydrogens are well protected against HX (Pf > 10^3), whereas others are much less so (Pf < 50). These peptides span a helix boundary. Near the N terminus, five residues located within the segment 1–10 are unprotected against HX as reported and discussed in detail before for apoA-I in the lipid-free state (19). Residues 8, 9, and 10 form the first turn of helix 1 with amide hydrogens not protected by a hydrogen bond acceptor. Residue 11 is the first protected amide hydrogen in helix 1, hydrogen-bonded to the main chain carbonyl of Pro 7 (i to i-4). The mean Pf for the slowly exchanging hydrogens in the N-terminal helix is 3,600, indicating a helical length with stabilization free energy of 5 kcal/mol. Similar considerations can be applied to the HX data for C-terminal peptides. The C-terminal peptide encompassing residues 236–243 exhibits low protection (Pf = 35) (Table S1) consistent with relatively unstable structure. Peptides 234–243, 231–243, and 230–243 contain progressively more amide hydrogens exhibiting greater protection (mean Pf = 1,200), consistent with the existence of a final length of stable helix terminating around residue 236.

In the 9.6-nm HDL particle at 5 °C, the HX kinetics are sufficiently slow that complete time courses can be obtained (Fig. S3). At 25 and 37 °C exchange is more rapid (Figs. S4 and S5). The effect of increasing temperature is illustrated for peptide 159–178 (Pf approximately 500 at 5 °C; Table S1) in Fig. S5. The Pf decreases to approximately 200 at 25 °C; at 37 °C exchange is essentially complete within 3 min. Nonetheless, the 25 °C time courses are broadly consistent with the 5 °C data, indicating that the conformation of apoA-I in the 9.6-nm discoidal HDL particle is similar at these temperatures.

ApoA-I Helix Properties in HDL Particles. Fig. 2 summarizes the complete analysis of the Pf values measured for apoA-I in a 9.6-nm discoidal HDL particle at pD 7.3, 5 °C. In *A*, the stabilization free energy against cooperative unfolding for each helical length is plotted against position in the apoA-I amino acid sequence [$\Delta G = -RT \ln K_{op}$ (where K_{op} is the fraction of time unfolded) = RT ln Pf; see *Materials and Methods* and *SI Text*]. In the lipid-associated state, apart from the N-terminal 6 residues and C-terminal 7 residues, the apoA-I molecule forms α-helical segments with free energies of stabilization in the range 3–5 kcal/mol. In lipid-free apoA-I the helical segments have similar ΔG [3.3–5.3 kcal/mol (19)], but large segments of the protein do not form α-helix and are disordered (ΔG ≤ 1.0 kcal/mol) (Fig. 2*A*). Upon binding to PL in the 9.6-nm HDL particle, the latter segments are induced to form α-helix with a gain in stabilization free energy of 2–4 kcal/mol. The locations of the α-helical segments in the lipid-bound and lipid-free apoA-I molecule are compared in Fig. 2 *B* and *C*.

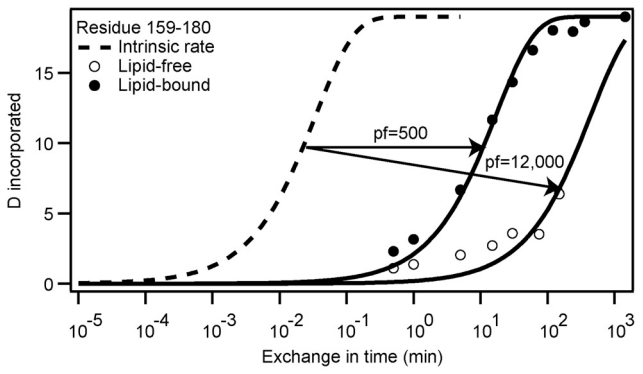

Fig. 1. Comparison of HX kinetics (pD 7.3, 5 °C) for peptide fragment 159–180 from the LCAT binding domain of apoA-I in lipid-free (○) and lipid-bound (9.6 nm discoidal HDL particle) states (●). The intrinsic rate (---) is the expected HX rate of the amide protons if the segment were random coil. The lipid-bound and lipid-free data are fitted to monoexponential kinetic curves. The calculated Pf values are indicated.

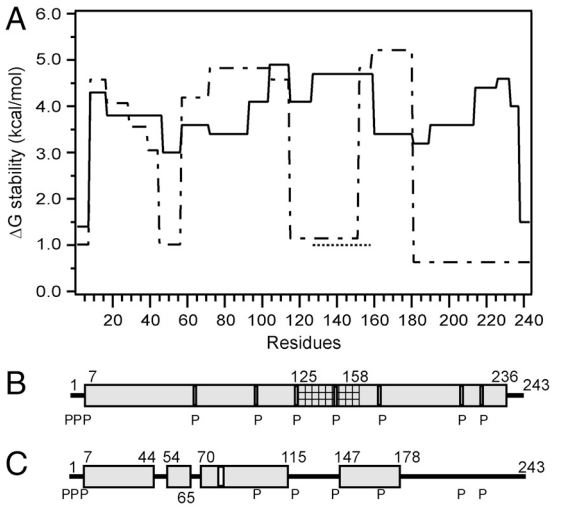

Fig. 2. Summary of the HX-derived secondary structure assignments and α-helix stabilities for apoA-I in lipid-free and lipid-bound (9.6-nm discoidal HDL particle) states. (*A*) Site-resolved stability of lipid-free (dashed line) (from ref. 19) and lipid-bound (solid line) apoA-I. The HX kinetic data (pD 7.3, 5 °C) for the 9.6-nm discoidal HDL particle in Fig. S3 and Table S1 were analyzed to obtain Pf values for each apoA-I peptide. Residues 125–158 (cross-hatched in *B*) exhibit bimodal HX kinetics (see Fig. S8) indicating two populations undergoing HX at different rates; the $\Delta G_{stability}$ for both states is shown (the dotted line at ΔG approximately 1 kcal/mol represents the fast state; see *text*). The disordered loop structure formed by the region around residues 125–158 is not included in *B*. *B* and *C* compare the HX-derived helix locations in lipid-bound (9.6-nm discoidal HDL particle) and lipid-free apoA-I, respectively. The gray cylinders represent α-helices, and the lines indicate disordered secondary structure. The positions of proline residues (P), whose presence leads to some perturbation of α-helix organization, are marked.

The analysis of helix properties summarized in Fig. 2 applies to apoA-I in a 9.6-nm discoidal HDL particle with a composition of approximately 70/1 mol/mol POPC/apoA-I. Incorporation of 10 mol% cholesterol has no significant effect on the HX kinetics (Fig. S6). Helix stability is also not changed by alterations in PC acyl chain composition; the apoA-I HX kinetics are essentially the same for HDL particles reconstituted with either POPC or dimyristoyl PC (Fig. S7).

It is noteworthy that certain helical segments become destabilized upon incorporation into an HDL particle. Helices in the regions of residues 60–100 and 150–180 possess ΔG values some 1–2 kcal/mol lower when lipid-bound than when lipid-free (Fig. 2*A*). This effect is demonstrated in detail in Fig. 1 for peptide 159–180. This peptide is of particular interest because it spans the region of the apoA-I molecule involved in the activation of the enzyme lecithin-cholesterol acyltransferase (LCAT) (25). Pf decreases from a value of 12,000 in the lipid-free state to 500 in the HDL particle. This observation is consistent with a prior report (26) showing that protection against HX in this segment is reduced in the HDL particle. However, the present results show that the segment 159–180 remains helical in the HDL particle and does not form a disordered loop protruding from the surface of the disc, as suggested before (26).

Bimodal HX Kinetics. For apoA-I in 9.6-nm discoidal HDL particles, the isotopic envelopes for peptide fragments between residues 125–158 (125–147, 125–158, 127–158, and 137–158) measured at HX times in the 30-s to 15-min range at 5 °C exhibit obvious bimodal distributions (Fig. S8). The segment of apoA-I monitored by peptide 125–158 (Fig. S8) is distributed in a 4/1 ratio between the slowly and rapidly exchanging populations, with exchange to the fully deuterated state not being complete in 240 min. The slow state has Pf = 5,000 (Table S1) corresponding to ΔG approximately 4.7 kcal/mol indicating relatively stable helix (cf. Fig. 2*A*). In contrast, most amides in the fast state have Pf < 10, indicating a disordered state. These results show that within the region of residues 125–158 the molecule occupies co-existing helical and disordered states. Interchange between the two states is on the time scale of tens of minutes (Fig. S8).

Effect of HDL Particle Size. The HX data in Fig. 3, Fig. S8, and Table S2 provide information on the helix properties of apoA-I in 7.8-nm discoidal HDL particles containing 28/1 mol/mol POPC/apoA-I. In contrast to the situation with 9.6-nm discs where most of the apoA-I molecule exhibits uniformly high protection and unimodal HX kinetics, accommodation of two apoA-I molecules at the edge of the smaller particle leads to many more segments exhibiting bimodal HX kinetics. The HX data for all apoA-I peptide fragments listed in Figs. S9 and S10 and Table S2 were analyzed in detail as described in *SI Results and Discussion*. Helix stabilities and relative occupancies of the fast and slow states for segments along the length of the entire apoA-I molecule are summarized in Fig. 3 *A* and *B*, respectively.

For the 7.8-nm disc, it can be estimated that the total number of amide hydrogens with Pf ≤ 10 is 43 (Table S2), which corresponds to a nonhelical content of about 18%, consistent with the CD spectrum (Fig. S2). The assignment of Pf ≥ 10 for helical structure also gives agreement between the HX- and CD-derived estimates of helix content in lipid-free apoA-I (19). Compared to amide hydrogens in unconstrained random coil that have expected Pf = 1 (23), unprotected (non-H-bonded) amide hydrogens on nonhelical but ordered segments exchange more slowly and have been seen to exhibit Pf values in the range 2–40 (27). Because the Pf for helical apoA-I amide hydrogens has to be set at >50 in order for the HX determination of apoA-I helix content in the 9.6-nm HDL particle to agree with the CD determination of 80% (Fig. S2), it follows that the nonhelical segments are likely

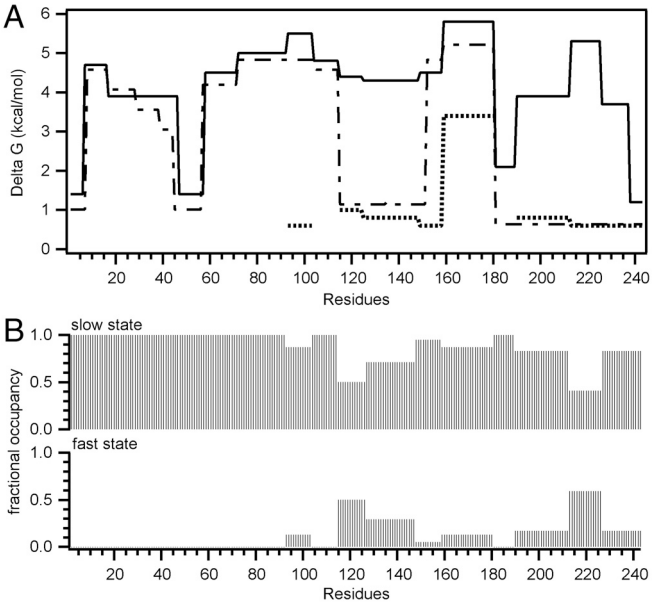

Fig. 3. HX kinetics (pD 7.3, 5 °C) for lipid-bound apoA-I in 7.8 nm POPC/apoA-I discoidal HDL particles. (*A*) Each segment of the plot of helix stabilization free energy against apoA-I sequence position corresponds to peptides shown in Fig. S9. For peptides exhibiting bimodal HX kinetics, ΔG for the fast and slow states are represented by the dotted and solid lines, respectively. The dashed line shows ΔG for lipid-free apoA-I. (*B*) Fractional occupancies for peptides exhibiting bimodal HX kinetics, calculated from 30 s HX data (cf. Fig. S8) of the fast and slow states.

to be significantly constrained. This effect probably reflects the close apoA-I—bilayer edge relationship.

Discussion

Effects of Association with PL on ApoA-I Structure. CD measurements have established that the transition of apoA-I from the lipid-free to the lipid-bound state is accompanied by an increase in α-helix content from about 50% to 80% (28, 29). Fig. S2 illustrates this effect for the 9.6-nm HDL particle in which each apoA-I molecule interacts with a proportionate amount of PL (70/1 mol/mol PL/apoA-I). The HX results specify the human apoA-I residues (45–53, 66–69, 116–146, and 179–236) that transition from random coil to helix upon incorporation into the 9.6-nm HDL disc (Fig. 2). The conformational change of these 102 residues corresponds to an increase in helix content of approximately 40%, a little higher than the value indicated by CD. The major contribution to helix formation comes from the C-terminal domain spanning residues 180–243, in agreement with prior EPR experiments (30). ApoA-I binds to a PL surface in a two-step mechanism in which an initial interaction mediated by the C-terminal domain is followed by opening of the N-terminal helix bundle (3, 10, 31). The results in Fig. 2 indicate that the latter step is accompanied by widespread helix formation. The formation of α-helix in the N- and C-terminal domains promotes high affinity binding of apoA-I to lipids; the approximately 30% increase in α-helix content contributes about 2.5 kcal/mol to the favorable free energy of binding (10, 29).

The apoA-I helical segments in both the 7.8- and 9.6-nm HDL discs exhibit free energies of stabilization in the range 3 to 5 kcal/mol (Figs. 2*A* and 3*A*), which is similar to the range measured by HX for lipid-free apoA-I (19). This observation is consistent with the results of chemical denaturation experiments (28, 32) showing that incorporation of apoA-I into discoidal HDL particles does not significantly affect the average α-helix stability. Individual helices variously exhibit stabilization and destabilization when relocated from the lipid-free state to the HDL-associated state (Fig. 2*A* and 3*A*). This observation indicates that

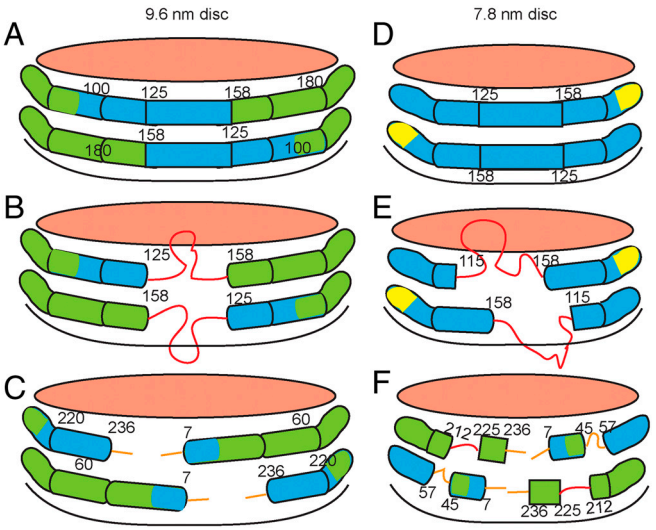

Fig. 4. Diagram comparing the secondary structures of apoA-I molecules in 9.6-nm (*A–C*) and 7.8-nm (*D–F*) discoidal HDL particles, as determined by HX/MS. The amphipathic α-helices are represented by cylinders colored according to their stability (Figs. 2*A* and 3*A*). The values of the free energy of stabilization (kcal/mol) are: red, ≤1; orange, 1–2; yellow, 2–3; green, 3–4; blue >4. The pink surfaces of the discs are covered by PL polar groups. The apoA-I molecules are organized according to the simple "double-belt" model (14) and any folding back or overlap of the ends of the apoA-I molecules (16, 35) is not demonstrated. *A* and *B* show the slow and fast states in which residues 125–158 adopt α-helical and disordered loop conformations, respectively. The diagrams show the two apoA-I molecules on each disc acting in concert and adopting the same conformation, but the segment spanning residues 125–158 also could be α-helical in one molecule and loop in the other. The orientation in *C* is obtained by a 180° clockwise rotation of the disc in *A* and depicts the nonhelical structures formed by the 6 or 7 amino acids at the ends of the apoA-I molecules. *D–F* show the equivalent information for a 7.8-nm discoidal HDL particle. The approximately 20% smaller area available at the edge of the 7.8-nm disc leads to displacement of about 20% more apoA-I amino acid residues from contact with PL molecules and enhances formation of protruding disordered loops (red in *E* and *F*). The regions of the apoA-I molecule that form these loops correspond to the nonhelical segments of the protein when it is in the lipid-free state. The surface-dissociated and surface-associated states co-exist on the time scale of minutes or longer; the degree of occupancy of these states varies along the lengths of the apoA-I molecules. As examples, segments spanning residues 115–158 and 212–225 form the depicted protruding structures 30–60% of the time in the 7.8-nm HDL particles (*E* and *F*; see *text* for further details). The diagrams are not to scale except for the relative major diameters of the two sizes of HDL discs.

there is no dominant effect of interfacial environment on helix stability (and HX rate) (also see section on hydrogen exchange in *SI Text*). The free energies of apoA-I helix stabilization in the lipid-free and lipid-bound states are significantly lower than values in the range 5–10 kcal/mol typically observed for globular proteins. The low global stability of the apoA-I molecule is consistent with high conformational flexibility. The stabilization free energies of 3–5 kcal/mol correspond to an unfolding equilibrium constant of approximately 10^{-3} meaning that the apoA-I α-helices in the surface of an HDL particle spend about 0.1% of the time unfolded. Because α-helix folding can occur on a sub-millisecond time scale, the α-helices in apoA-I (lipid-free and lipid-associated) probably unfold (and refold) on a time scale of seconds or faster (19). This dynamic behavior and structural flexibility of apoA-I facilitates the remodeling of HDL particles (33), which is critical for their maturation and metabolism.

Secondary Structure of ApoA-I in Discoidal HDL Particles of Different Sizes. The most widely accepted model for the structure of a 10-nm-diameter reconstituted HDL particle is one in which the apoA-I molecules adopt the so called "double-belt" organization (14). Despite some disagreement (34), the particle is thought to be discoidal in shape and to contain two equivalent apoA-I molecules arranged as continuous antiparallel helices around the edge of a segment of PL bilayer. Chemical cross-linking and mass spectrometry studies are consistent with this structure and have shown that a central helical segment (residues 121–142) in one apoA-I molecule is packed adjacent to the same segment in its partner (reviewed in refs. 4, 5). Because available crystal structures are for truncated lipid-free apoA-I variants, models of the organization of the terminal regions are less well developed although there is evidence that the N-terminal region is folded back on itself (5, 16). It is known that apoA-I conformation is sensitive to changes in HDL particle size and, to account for this effect, structural models containing either variations in N- and C-terminal packing or helix-loop transitions have been proposed (35–39). However, in the absence of a detailed and complete description of apoA-I secondary structure in HDL particles, the validity of such concepts remains uncertain. The information about α-helix locations and stabilities generated by the present HX study allows detailed evaluation of models of apoA-I organization in such particles.

9.6-nm Discoidal HDL. The distribution of α-helices in lipid-associated apoA-I in a 9.6-nm discoidal HDL particle (Fig. 2*B*) demonstrates that apoA-I adopts a continuous extended α-helical conformation essentially throughout its whole length, excepting only residues 1–6 and 237–243. This observation is consistent with inferences from structure prediction algorithms (13) and with the crystal structures of truncated apoA-I variants in the lipid-free state (15, 16). The level of protection against HX is consistent with stable helix formation. EPR methods have been utilized to examine the secondary structure of apoA-I residues 6–98 and 163–241 in similar discoidal HDL particles (30, 40, 41). Consistent with the HX result (Fig. 2*B*), segments spanning residues 6–34, 50–98, and 185–233 were found to adopt α-helix. However, the EPR finding that residues 35–39 are unstructured and residues 234–243 are helical is inconsistent with HX results summarized in Fig. 2*B*. These discrepancies may arise from the use of apoA-I fragments in the EPR experiments. In the double-belt model of 10-nm-diameter HDL discs, it is clear that the apoA-I molecules must extend around the circumference of the particle and interact with the PL acyl chains at the edge of the disc to shield them from exposure to the aqueous phase (14). Thus, the helical secondary structure shown in linear form in Fig. 2*B* is in fact curved due to (*i*) kinking at the proline residues and (*ii*) the intrinsic curvature of amphipathic α-helices (42). Proline residues are frequently located at the N terminus of α-helical segments (43), and the positions of these sites are indicated in Fig. 2*B*. The HX results indicate that the occurrence of a proline residue does not lead to the appearance of unprotected amide hydrogens. This is consistent with proline residues in helices causing only minimal disruption of hydrogen bonding (typically involving loss of only the N_{i+1}–O_{i-3} hydrogen bond) (42).

The segment of the lipidated apoA-I molecule spanning residues 125–158 exhibits bimodal HX kinetics (Fig. S8), indicating that this region of the protein exists in two physical states with conformational exchange between them at 5 °C occurring on the time scale of tens of minutes. This result is consistent with prior findings (36–39, 44, 45) that this segment of the apoA-I molecule can form a hinge domain or loop, with residues either in direct contact with the PL molecules at the edge of the disc or protruding into the aqueous phase. This region of the apoA-I molecule is apparently particularly flexible; X-ray crystallography has shown that residues 121–142 form the most flexible part of the half-circle dimer structure adopted by C-terminally truncated apoA-I (16). The slow state detected by HX presumably represents helical segments bound to the edge of the disc. The presence of unprotected amide hydrogens in the fast state is consistent with the existence of a desorbed, disordered loop. Thus, the segment

around residues 125–158 most likely forms a loop domain containing proline residue 143. The relative occupancy of this loop structure is about 20% at 5 °C. The HX data indicate that any given apoA-I segment behaves equivalently in all HDL particles present in the homogeneous population.

7.8-nm Discoidal HDL. Relative to the 9.6-nm disc (70/1 mol/mol POPC/apoA-I), the 7.8-nm disc (28/1 mol/mol POPC/apoA-I) has fewer PL acyl chains that require protection from exposure to the aqueous phase by interaction with the amphipathic α-helices of apoA-I. There are some morphological differences between the two sizes of HDL particles (46, 47), but to a first approximation both can be considered as discs so that the 7.8-nm particle has an approximately 20% smaller perimeter. It follows that the two apoA-I molecules accommodated around the edge of a 7.8-nm disc are relatively crowded, compared to the 9.6-nm disc. The HX data reveal that this crowding leads to the apoA-I molecules sampling different physical states with various segments either on or off the 7.8-nm particle surface. Importantly, the approximately 20% reduction in available surface area leads to a measured 18% decrease in the fraction of apoA-I residues in direct contact with PL molecules at the disc edge [calculated from the occupancy of the fast-exchanging, less-protected, state in peptides that exhibit bimodal HX kinetics, including the disordered residues 45–57 (Fig. 3)]. These different apoA-I conformations co-exist on the time scale of tens of minutes. The structural perturbation caused by molecular crowding at the edge of the 7.8-nm disc is experienced unevenly along the length of the apoA-I molecules. As summarized in Fig. 3*C*, the N-terminal residues 1–90 occupy a single physical state (unimodal isotopic envelopes) whereas C-terminal segments (residues 90–243) occupy two physical states. In these cases the occupancy of the desorbed state ranges from as low as 5% for some segments to as high as 60%. These occupancies can be considered to correspond to relative concentrations and to relative lifetimes.

The organization and properties of the helical segments of the apoA-I molecules in 7.8- and 9.6-nm discoidal HDL particles are shown schematically in Fig. 4. An important novel structural insight is that, on a given size of HDL particle, various segments along the apoA molecule equilibrate between the desorbed and adsorbed states. It is noteworthy that the segments of the apoA-I molecule that form disordered structure in the 7.8-nm HDL particle (residues 45–57, 115–158, 190–243) (Fig. 3*B*) are mostly those that are nonhelical in lipid-free apoA-I (Fig. 2*C*). Apparently, the propensity of these regions to maintain disordered configurations in lipid-free apoA-I similarly favors disordered loop structures in the lipid-bound state. The finding that residues 115–158 readily desorb from the disc edge is consistent with other spectroscopic results showing that residues 130–170 (37) and residues 133–146 (38) form flexible loops.

The minimum in system free energy associated with the selective formation of HDL discs with 9.6-nm diameter probably reflects the optimized coverage of the hydrophobic surface formed by POPC acyl chains achieved by the two maximally α-helical apoA-I molecules. The propensity of the nonhelical segments in the lipid-free apoA-I molecule to form unstructured loops is likely to be the basis for the minimum in free energy associated with selective formation of the 7.8-nm HDL disc where the same segments form helices and loops (Fig. 4). Formation of two alternative states by these regions of the apoA-I molecule could provide additional free energy of stabilization for the small disc (48).

Materials and Methods

Homogeneous reconstituted HDL particles (9.6- and 7.8-nm hydrodynamic diameter) containing POPC and human apoA-I were prepared by the cholate dialysis method (49). The apoA-I secondary structure in these particles was investigated using an HX with fragment-separation (50) MS analysis (17, 51). Mass spectra were analyzed using in-house software ExMS (18). Time-dependent HX experiments were performed at pD 7.3 (5, 25, and 37 °C). As summarized in Fig. 1, the observed HX rate curve (k_{obs}) for each peptide fragment was compared to a reference (intrinsic) rate (k_{ref}) expected for the peptide in a random coil state (23, 52). The HX protection factor $Pf(= k_{ref}/k_{obs})$ for each peptide was used to calculate the free energy of stabilization against helix unfolding ($\Delta G = RT \ln Pf$). Further details about interpretation of HX data are in *SI Text*.

ACKNOWLEDGMENTS. This work was supported by National Institutes of Health Grants HL22633 (M.C.P.) and GM031847 (S.W.E.).

1. Atkinson D, Small DM (1986) Recombinant lipoproteins: Implication for structure and assembly of native lipoproteins. *Annu Rev Biophys Biophys Chem* 15:403–456.
2. Pownall HJ, Massey JB, Sparrow JT, Gotto AM (1987) Lipid–protein interactions and lipoprotein reassembly. *Plasma Lipoproteins*, ed AM Gotto (Elsevier Science Publishers B.V, Amsterdam), pp 95–127.
3. Brouillette CG, Anantharamaiah GM, Engler JA, Borhani DW (2001) Structural models of human apolipoprotein A-I: A critical analysis and review. *Biochim Biophys Acta* 1531:4–46.
4. Davidson WS, Thompson TB (2007) The structure of apolipoprotein A-I in high density lipoproteins. *J Biol Chem* 282:22249–22253.
5. Thomas MJ, Bhat S, Sorci-Thomas MG (2008) Three-dimensional models of HDL apoA-I: Implications for its assembly and function. *J Lipid Res* 49:1875–1883.
6. Huang R, et al. (2011) Apolipoprotein A-I structural organization in high-density lipoproteins isolated from human plasma. *Nat Struct Mol Biol* 18:416–422.
7. Lund-Katz S, Phillips MC (2010) High density lipoprotein structure-function and role in reverse cholesterol transport. *Subcell Biochem* 51:183–227.
8. Rye KA, Bursill CA, Lambert G, Tabet F, Barter PJ (2009) The metabolism and anti-atherogenic properties of HDL. *J Lipid Res* 50:S195–S200.
9. Duong PT, et al. (2006) Characterization of nascent HDL particles and microparticles formed by ABCA1-mediated efflux of cellular lipids to apoA-I. *J Lipid Res* 47:832–843.
10. Saito H, Lund-Katz S, Phillips MC (2004) Contributions of domain structure and lipid interaction to the functionality of exchangeable human apolipoproteins. *Prog Lipid Res* 43:350–380.
11. Zannis VI, Chroni A, Krieger M (2006) Role of apoA-I, ABCA1, LCAT, and SR-BI in the biogenesis of HDL. *J Mol Med* 84:276–294.
12. Vedhachalam C, et al. (2007) Mechanism of ATP-binding cassette transporter A1-mediated cellular lipid efflux to apolipoprotein A-I and formation of high density lipoprotein particles. *J Biol Chem* 282:25123–25130.
13. Segrest JP, et al. (1992) The amphipathic helix in the exchangeable apolipoproteins: A review of secondary structure and function. *J Lipid Res* 33:141–166.
14. Segrest JP, et al. (1999) A detailed molecular belt model for apolipoprotein A-I in discoidal high density lipoprotein. *J Biol Chem* 274:31755–31758.
15. Borhani DW, Rogers DP, Engler JA, Brouillette CG (1997) Crystal structure of truncated human apolipoprotein A-I suggests a lipid-bound conformation. *Proc Natl Acad Sci USA* 94:12291–12296.
16. Mei X, Atkinson D (2011) Crystal structure of C-terminal truncated apolipoprotein A-I reveals the assembly of high density lipoprotein (HDL) by dimerization. *J Biol Chem* 286:38570–38582.
17. Mayne L, et al. (2011) Many overlapping peptides for protein hydrogen exchange experiments by the fragment separation-mass spectrometry method. *J Am Soc Mass Spectrom* 22:1898–1905.
18. Kan ZY, Mayne L, Sevugan Chetty P, Englander SW (2011) ExMS: Data analysis for HX-MS experiments. *J Am Soc Mass Spectrom* 22:1906–1915.
19. Chetty PS, et al. (2009) Helical structure and stability in human apolipoprotein A-I by hydrogen exchange and mass spectrometry. *Proc Natl Acad Sci USA* 106:19005–19010.
20. Jonas A, Wald JH, Toohill KL, Krul ES, Kezdy KE (1990) Apolipoprotein A-I structure and lipid properties in homogeneous, reconstituted spherical and discoidal high density lipoproteins. *J Biol Chem* 265:22123–22129.
21. Davidson WS, Silva RAG (2005) Apolipoprotein structural organization in high density lipoproteins: Belts, bundles, hinges and hairpins. *Curr Opin Lipidol* 16:295–300.
22. Cavigiolio G, et al. (2008) The interplay between size, morphology, stability, and functionality of high-density lipoprotein subclasses. *Biochemistry* 47:4770–4779.
23. Bai Y, Milne JS, Mayne L, Englander SW (1993) Primary structure effects on peptide group hydrogen exchange. *Proteins* 17:75–86.
24. Englander SW, Kallenbach NR (1983) Hydrogen exchange and structural dynamics of proteins and nucleic acids. *Q Rev Biophys* 16:521–655.
25. Sorci-Thomas MG, Bhat S, Thomas MJ (2009) Activation of lecithin: Cholesterol acyltransferase by HDL ApoA-I central helices. *Clin Lipidol* 4:113–124.
26. Wu Z, et al. (2007) The refined structure of nascent HDL reveals a key functional domain for particle maturation and dysfunction. *Nat Struct Mol Biol* 14:861–868.
27. Skinner JJ, Lim WK, Bedard S, Black BE, Englander SW (2012) Protein hydrogen exchange: Testing current models. *Protein Sci*, in press.
28. Sparks DL, Lund-Katz S, Phillips MC (1992) The charge and structural stability of apolipoprotein A-I discoidal and spherical recombinant high density lipoprotein particles. *J Biol Chem* 267:25839–25847.
29. Saito H, et al. (2004) Alpha-helix formation is required for high affinity binding of human apolipoprotein A-I to lipids. *J Biol Chem* 279:20974–20981.
30. Oda MN, Forte TM, Ryan RO, Voss JC (2003) The C-terminal domain of apolipoprotein A-I contains a lipid-sensitive conformational trigger. *Nat Struct Biol* 10:455–460.

31. Saito H, et al. (2003) Domain structure and lipid interaction in human apolipoproteins A-I and E: A general model. *J Biol Chem* 278:23227–23232.
32. Reijngoud DJ, Phillips MC (1982) Mechanism of dissociation of human apolipoprotein A-I from complexes with dimyristoylphosphatidylcholine as studied by guanidine hydrochloride denaturation. *Biochemistry* 21:2969–2976.
33. Guha M, Gao X, Jayaraman S, Gursky O (2008) Correlation of structural stability with functional remodeling of high-density lipoproteins: The importance of being disordered. *Biochemistry* 47:11393–11397.
34. Jones MK, et al. (2010) Assessment of the validity of the double superhelix model for reconstituted high density lipoproteins: A combined computational-experimental approach. *J Biol Chem* 285:41161–41171.
35. Bhat S, Sorci-Thomas MG, Tuladhar R, Samuel MP, Thomas MJ (2007) Conformational adaptation of apolipoprotein A-I to discretely sized phospholipid complexes. *Biochemistry* 46:7811–7821.
36. Li L, et al. (2004) Double belt structure of discoidal high density lipoproteins: Molecular basis for size heterogeneity. *J Mol Biol* 343:1293–1311.
37. Maiorano JN, Jandacek RJ, Horace EM, Davidson WS (2004) Identification and structural ramifications of a hinge domain in apolipoprotein A-I discoidal high-density lipoproteins of different size. *Biochemistry* 43:11717–11726.
38. Martin DD, Budamagunta MS, Ryan RO, Voss JC, Oda MN (2006) Apolipoprotein A-I assumes a "looped belt" conformation on reconstituted high density lipoprotein. *J Biol Chem* 281:20418–20426.
39. Li L, Li S, Jones MK, Segrest JP (2012) Rotational and hinge dynamics of discoidal high density lipoproteins probed by interchain disulfide bond formation. *Biochim Biophys Acta* 1821:481–489.
40. Lagerstedt JO, et al. (2011) Structure of apolipoprotein A-I N terminus on nascent high density lipoproteins. *J Biol Chem* 286:2966–2975.
41. Lagerstedt JO, Budamagunta MS, Oda MN, Voss JC (2007) EPR spectroscopy of site-directed spin labels reveals the structural heterogeneity in the N-terminal domain of apo AI in solution. *J Biol Chem* 282:9143–9149.
42. Barlow DJ, Thornton JM (1988) Helix geometry in proteins. *J Mol Biol* 201:601–619.
43. Piela L, Nemethy G, Scheraga HA (1987) Proline-induced constraints in alpha-helices. *Biopolymers* 26:1587–1600.
44. Cheung MC, et al. (1987) Characterization of high density lipoprotein subspecies: Structural studies by single vertical spin ultracentrifugation and immunoaffinity chromatography. *J Lipid Res* 28:913–929.
45. Calabresi L, Meng QH, Castro GR, Marcel YL (1993) Apolipoprotein A-I conformation in discoidal particles: Evidence for alternate structures. *Biochemistry* 32:6477–6484.
46. Gu F, et al. (2010) Structures of discoidal high density lipoproteins: A combined computational-experimental approach. *J Biol Chem* 285:4652–4665.
47. Miyazaki M, Nakano M, Fukuda M, Handa T (2009) Smaller discoidal high-density lipoprotein particles form saddle surfaces, but not planar bilayers. *Biochemistry* 48:7756–7763.
48. Sharp KA, Englander SW (1994) How much is a stabilizing bond worth? *Trends Biochem Sci* 19:526–529.
49. Matz CE, Jonas A (1982) Micellar complexes of human apolipoprotein A-I with phosphatidylcholines and cholesterol prepared from cholate-lipid dispersions. *J Biol Chem* 257:4535–4540.
50. Englander JJ, Rogero JR, Englander SW (1985) Protein hydrogen exchange studied by the fragment separation method. *Anal Biochem* 147:234–244.
51. Zhang Z, Smith DL (1993) Determination of amide hydrogen exchange by mass spectrometry: A new tool for protein structure elucidation. *Protein Sci* 2:522–531.
52. Connelly GP, Bai Y, Jeng MF, Englander SW (1993) Isotope effects in peptide group hydrogen exchange. *Proteins* 17:87–92.